Postprint of: Ryl J., Burczyk Ł., Bogdanowicz R., Sobaszek M., Darowicki K., Study on surface termination of boron-doped diamond electrodes under anodic polarization in H_2SO_4 by means of dynamic impedance technique, Carbon, Vol. 96 (2016), pp. 1093-1105, DOI: 10.1016/j.carbon.2015.10.064

Study on surface termination of boron-doped diamond electrodes under anodic polarization in H_2SO_4 by means of dynamic impedance technique

Jacek Ryl[a]*, Lukasz Burczyk[a], Robert Bogdanowicz[b], Michal Sobaszek[b], Kazimierz Darowicki[a]

[a] *Department of Electrochemistry, Corrosion and Materials Engineering, Faculty of Chemistry, Gdansk University of Technology, 11/12 Narutowicza St., 80-233 Gdansk, Poland*
[b] *Department of Metrology and Optoelectronics Faculty of Electronics, Telecommunications and Informatics, Gdansk University of Technology, 11/12 G. Narutowicza St., 80-233 Gdansk, Poland*

Abstract

Anodic oxidation is a popular way to modify termination bonds at boron doped diamond electrodes altering their electrochemical and physicochemical properties. Our studies, performed with dynamic electrochemical impedance spectroscopy technique, supported with X-ray photoelectron spectroscopy and ellipsometry analysis prove its utility in continuous on-line monitoring of impedance changes on the electrode surface under polarization conditions, which may be of great use for the optimization of working conditions of the process. Based on our results, it can be observed that oxidation of termination bonds is a multistep process, each stage initiated at different anodic polarization potential. The factors influencing oxidation of termination bonds are presented and discussed. It was also possible to draw a conclusion about the removal of sp^2 carbon impurities from the electrode surface as a precondition to activate the oxidation process. The depth and time of polarization, boron uptake at the grain boundaries, as well as crystallographic orientation of individual grains influence the heterogeneity of the oxidation process. Its partial reversibility was observed as a result of cathodic polarization in the range of hydrogen evolution, however due to irreversible corrosion of sp^2 impurities, hydrogenation is not complete. This form of hydrogenation additionally contaminates the electrode surface with sulphur.

*Corresponding author. Tel: +48 583471092. E-mail: jacek.ryl@pg.gda.pl (J. Ryl)

1. Introduction

In a couple of years, boron-doped diamonds (BDD) might become one of the most challenging electrode material. This phenomena is based on their unique properties e.g. wide potential window, high anodic stability, inertness in harsh environment, chemical and mechanical durability. The electrochemical properties of diamond electrodes were found to be quite sensitive to surface termination. External termination bonds in diamond electrodes also defines physical and chemical properties and as such are an important factor, deciding about possible applications and performance of BDD electrodes. Hydrogen termination of boron doped diamond (HT-BDD) leads to non-polar, hydrophobic surface with high conductivity and low charge transfer resistance. On the other hand, oxygen terminated boron doped diamond electrodes (OT-BDD) are hydrophilic, polar and manifest lower electric conductivity [1,2].

Conversion from HT-BDD to OT-BDD could be carried out in several ways. Oxygen plasma, ozone treatment, wet chemical oxidation, ultraviolet radiation, exposure to high temperatures and electrochemical anodic polarization have been reported as oxidation agents of H-terminated BDD polycrystalline electrodes. Denisenko *et al.* [3] confirmed that different oxidation methods lead to different termination and as such to different activity of BDD electrodes. Boukherroub *et al.* [4] have shown that UV irradiation of HT-BDD films in ambient air leads to surface oxidation, dominated by hydroxyl groups. Wang *et al.* [5] performed studies on the amount of hydroxyl/carbonyl groups formed with electrochemical, ozone and photochemical oxidation methods and reported that the electrochemical oxidation results in the formation of the highest amount of C-OH groups. Much more aggressive oxidation is achieved by oxygen plasma treatment, leading to severe morphological changes not only for BDD but also diamond electrodes. Regardless of the oxidation method, the amount of carbonyl bonds is quite low. It has also been observed that the oxidation time results in a high increase of oxygen content, with preferential formation of C-O-C groups. Hoffmann *et al.* [6] performed atomic force microscopy (AFM) study of influence of polarization depth on the oxidation level of BDD electrodes, by selective attachment of nitrophenyl diazonium to H-terminated grains. They found out that oxidation level is determined by the oxidation voltage, and the process is still incomplete for potentials exceeding 6 V. It was also their finding that the oxidation process is heterogeneous in the nanometer scale.

There is a need to modify the surface of BDD electrodes due to the insufficiency of chemically reactive groups, which precludes the attachment of organic compounds to the electrode surface [7]. The formation of hydroxyl groups or carbonyl groups is desired, as well-known chemical routes can be used to link functional groups –OH or –COOH units. Different types of termination groups influence the durability and adhesion of those films. The most widely used approach to functionalizing diamond film surface with organic compounds is an amine functionality introduced to the surface. So far, several amination methods of diamond surface have been proposed [7-9]. In general they require: (I) etching by NH_3 plasma in a specific reactor [9], (II) chemical modification with (3-aminopropyl) triethoxysilane [10], (III) photochemical reaction of amino molecules containing a vinyl group [11], or (IV) diazonium functionalization [12]. Gu *et al.* [13] demonstrated a one-step chemical modification of BDD by the thin polyaniline/poly (acrylic acid) composite polymer film. The procedure did not show any non-specific DNA adsorption, and DNA probes immobilized on the BDD substrates were stable and selective to DNA sensing, while the oxidation peak potentials were lower than those reported for the oxidation of guanine and adenine on other carbon-based electrodes. Next, in a former study of plasma polymerized allyamine films, Bogdanowicz *et al.* [14] found that even a small increase of potential (0.2 V) within polarization range of transformation of termination groups may lead to almost complete detachment of the film from the electrode surface.

Thin BDD film contains a certain amount of graphite in its structure. The content of sp^2-hybridized bonds can be controlled by the CH_4/H_2 ratio in the reaction chamber during layer formation, and the amount of non-diamond phases increases with the admixture of CH_4. As the content of sp^2 carbon increases, the concentration of acceptors decreases [15,16]. Graphite participates in the charge transfer process on the electrode surface. An example being electrodes with high sp^3/sp^2 ratio oxidation of organic compounds that proceed more rapidly [17], where the high content of sp^2 carbon during application for water disinfection results in forming hazardous perchlorate species, in contrast to electrodes with higher content of sp^3 carbon for which perchlorate level is negligible. The removal of sp^2 contamination is possible by means of electrochemical treatment, where it corrodes and is etched away in the form of CO_2 [18-20]. On the other hand, some methods of oxidation can damage diamond surfaces, as in the case of high energy plasma treatment, leading to a higher level of carbon dimers or sp^2 phases appearance [5,21,22].

Properties of HT-BDD are subject to change as a result of aging of the electrode, induced even by an air-formed oxidation. Hydrogenation of termination bonds is possible by means of hydrogen plasma or hot filament treatments. Hoffmann *et al.* [23] suggest that it is possible to reverse the oxidation process also by means of electrochemical treatment, as a result of application of negative voltages in acidic solutions. Such a mechanism was proposed as hydrogen attachment via a production of hydrogen radicals. Hydrogenation of the BDD surface cannot be complete, due to the irreversible removal of sp^2 contamination during prior oxidation process.

In view of the above, it would be significant, both from a scientific and technological perspective, to define the working conditions leading to the most optimized results of the oxidation process. This paper focuses on determination of kinetics and mechanism of anodic oxidation of BDD electrodes in sulphuric acid environment by means of novel methodology – Dynamic Electrochemical Impedance Spectroscopy (DEIS). DEIS have been widely used in different areas of electrochemistry and corrosion science, for investigation and monitoring of non-stationary systems [24-26]. Based on this investigation, the fundamental understanding of the influence of polarization conditions on the electric behavior and the reversibility of the oxidation process will be studied.

2. Experimental

2.1. Si/BDD electrode preparation

The BDD electrodes were deposited in an microwave plasma-assisted chemical vapour deposition system (Seki Technotron AX5400S, Japan) on p-type Si substrates with (100) orientation. The substrates were cleaned by sonication in acetone and 2-propanol for 5 min in each solvent. Next, the substrates were seeded by means of spin-coating in a nanodiamond suspension (crystallite size of 5-10 nm), and spun three times for 60 sec at 4000 rpm. The temperature of the heating stage was kept at 700°C during the deposition process. In the first step of the procedure, the substrates were etched in hydrogen plasma for 1 min. The optimized power of microwave plasma for diamond synthesis was kept at 1300 W. The excited plasma was ignited by microwave radiation (2.45 GHz). The total flow of gas mixture, containing 1% of the molar ratio of CH_4-H_2, was kept at 300 sccm. All samples were doped by using diborane (B_2H_6) dopant precursor; the [B]/[C] ratio in the plasma was 10000 ppm resulting in acceptor concentration of 3×10^{21} cm^{-3} [27]. The reactor chamber was evacuated to a base

pressure of about 10^{-6} Torr, while the process pressure was kept at 50 Torr. The time of polycrystalline layer growth was 6h, which resulted in the thickness of the deposited films of approx. 2 μm.

Scanning electron microscopy (SEM) image of hydrogenated BDD surface at 10k B/C ratio exhibits homogeneous coverage of BDD crystallites on the surface of the electrode, as presented on Fig. 1. The surface is free from cracks and microdefects. The average crystallite size, around 800 nm, is in agreement with previous studies [28]. The inlet of the image shows that at several locations even smaller grains can be observed among the well-faceted diamond crystallites. Some crystallites have limited area of growth but it was additionally suggested by Santana *et al*. [29] that these grains may be associated with sp^2 micro-domains on the electrode surface. The grains are smaller due to higher boron incorporation. This theory is confirmed by a fact that average crystallite size decrease at high B/C ratios [28,30].

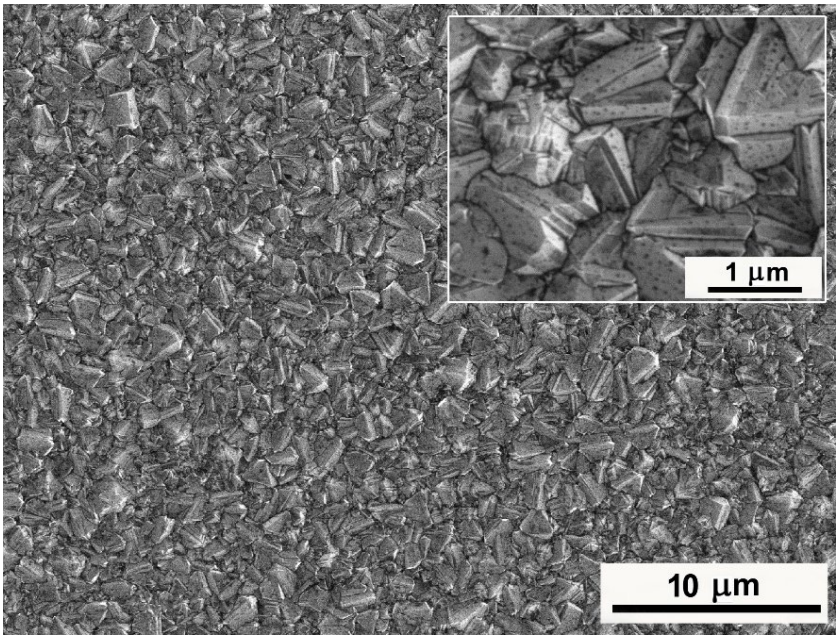

Fig. 1 – SEM micrograph of HT-BDD electrode subjected to investigation. Magnification x2k, inset magnification x20k. 20 kV accelerating voltage, secondary electrons mode.

2.2. Measurement techniques

Electrochemical modification: Surface modification through anodic oxidation as well as electrochemical investigation of Si/BDD electrode were carried out in a three-electrode cell, with $Ag|Ag_2SO_4$ reference electrode (+0.273 V vs SHE) and platinum mesh as counter

electrode. All potentials reported in the paper refer to this electrode. $Ag|Ag_2SO_4$ reference electrode was prepared to avoid chloride contamination from popular Ag|AgCl electrode, in accordance with methodology proposed by Velicky *et al*. [31]. Silver wire was pretreated by polishing and annealing in flame. Galvanostatic oxidation was conducted in 0.1 mol dm^{-3} sodium sulfate solution. Charge passed through 6 cm silver wire was equal to 1 C under current density of 1 x 10^{-5} A cm^{-2}. Volume of the electrochemical cell was 100 mL, ensuring constant electrolytic conditions throughout the measurement. The investigation was carried out in 1M H_2SO_4 solution. The sample area that was submitted to electrochemical investigation was 0.50 cm^2.

Surface modification of hydrogen terminated Si/BDD and its transform to OT-BDD was achieved by means of anodic polarization. Anodic oxidation of termination groups is an irreversible process, however certain studies were made, reporting on the partial restoration of electrochemical and physic-chemical properties of hydrogenated BDD electrode [23,32]. Cyclic voltammetry (CV) was used, with polarization range between -1.8 V to +2.5 V vs $Ag|Ag_2SO_4$. Cathodic polarization range was chosen to correspond to potentials of such re-transformation, according to Chaplin *et al*. [32], who suggested that atomic hydrogen produced by the Volmer discharge reaction can react with the surface C atoms. Anodic polarization range was chosen on the basis of previous studies, proven to be sufficient for OT-BDD transition [33]. CV studies were done for ten consecutive polarization cycles, at a rate of 1 mV/s.

Electrochemical study was performed on a measuring system consisting of Autolab 302N (Ecochemie, The Netherlands), for CV scans and PXI-4462 card operating in PXI-1031 chassis (National Instrument, USA) used for generation of AC perturbation signal as well as simultaneous recording of both voltage perturbation and current response signals.

DEIS methodology: DEIS is a variation of Electrochemical Impedance Spectroscopy (EIS), which omits some EIS restrictions and allows measurements under non-stationary conditions. The research object is excited simultaneously with a package of elementary signals, each described by its own amplitude, frequency and phase shift. This approach allows for significant reduction of the duration of measurement, which now depends only on the lowest frequency component (also reduced). It is possible to carry out DEIS simultaneously with DC measurements, such as cyclic voltammetry, thus providing more detailed knowledge about the investigated system. Analyzing the response with the use of Short - Time Discrete Fourier

Transformation (STDFT) provides location of impedance spectrum in time. More detailed information about DEIS methodology and setup can be found in the following references [24,34].

Dynamic impedance measurements were conducted for a frequency range between 4.5 kHz to 0.7 Hz. The sampling frequency of 128 kHz resulted from the measurement card settings. Multisinusoidal signal was composed of 20 sinusoids, with 5 points per decade of frequency. Peak-to-peak amplitude of the perturbation signal did not exceed 30 mV. The resulting signal was cut with an analyzing window of 10 seconds in length, and subjected to Fourier transformation using STDFT.

XPS analysis: Escalab 250Xi (ThermoFisher Scientific, United Kingdom) was used to carry out high-resolution photoelectron spectroscopy (XPS) measurements to determine chemical binding properties of the surface, utilizing monochromatic Al Kα source and a spot diameter of 650 μm, with charge neutralization implemented by means of a flood gun. High-resolution spectra were recorded at energy step size of 0.1 eV at a pass energy of 10 eV. Peak deconvolution and data analysis were performed using Avantage software supplied by the manufacturer.

Topography study: The morphology of the samples was characterized by S-3400N scanning electron microscope (Hitachi, Japan) equipped with a tungsten source. A secondary electron detector was used, analysis was performed under 20 kV accelerating voltage.

Surface wettability: Wettability angle was measured by the sessile drop method (drop volume ~50 μL) using the self-designed tensiometer system based on B/W CCD camera (Thorlabs, DCU223M, USA). Determination of the angle between the BDD surface and the tangent of the drop was performed using MATLAB 6.0 (The MathWorks, USA). The contact angle was measured in three different spots, and for both sides of the drop.

Spectroscopic Ellipsometry (SE): SE investigations were carried out with a phase-modulated ellipsometer Jobin-Yvon UVISEL (HORIBA Jobin-Yvon Inc., Edison, USA). The investigated wavelength range was 260 to 830 nm. The experiments were performed at room temperature using an angle of incidence fixed at 70º. Ellipsometric fitting was based on a three-phase optical model (air/surface roughness film (SRL)/ BDD). The 3-micrometer thick, highly boron-doped diamond films were considered as a substrate in the analyzed model in agreement with high optical absorption in investigated wavelength range. The top surface

roughness layer has been assumed as a composition of the BDD substrate with spaces filled with air. Such an approach allowed for the estimation of the average roughness of the films using the Bruggeman effective medium approximation (EMA). The BDD was expected to be an isotropic, homogeneous material and its dispersion was fitted to the Tauc-Lorentz oscillator (TL) model. This model was used recently for amorphous semiconductors by Gioti *et al*. [35] and Logothetidis *et al.* [36]. Such materials exhibit the presence of two separated contributions of inter-band electronic transition related to sp^2 and sp^3 bonded carbon [37]. The parameters of the TL model were fitted for each of the analyzed BDDs. Finally, the assumed optical model was fitted to the experimental data using the non-linear Levenberg-Marquardt regression method for mean-square error minimization (MSE) [38]. As a result of SE analysis, the thickness and optical constants, i.e. refractive index $n(\lambda)$ and extinction coefficient $k(\lambda)$ were obtained.

3. Results and discussion

3.1. Electrochemical modification of termination bonds

In order to determine various modification of BDD termination bonds as a result of anodic oxidation treatment, samples were investigated by means of cyclic voltammetry (CV) combined with DEIS study under different anodic polarization limit; +0.5, +1.4, +1.6, +1.9, +2.2 and +2.5 V vs $Ag|Ag_2SO_4$. Cathodic polarization limit was correlated with hydrogen evolution reaction and equal to -1.8 V vs $Ag|Ag_2SO_4$.

Figure 2 shows cyclic voltammetry (CV) results for the first and tenth polarization cycle, carried out for BDD electrode in 1M H_2SO_4 solution in the widest polarization range to +2.5 V vs $Ag|Ag_2SO_4$. A single peak can be observed on the anodic polarization curve, initiated at a value of potential 1.5 V with maximum at approx. 1.65 V vs $Ag|Ag_2SO_4$ and current densities in peak increasing with consecutive cycles. The anodic and cathodic peaks were split in a wide potential range, with cathodic peak present in the vicinity of potential of hydrogen evolution reaction (inset of Fig. 2). Large separation between the anodic and cathodic peaks indicates that the oxidation process is irreversible, and the oxidation/reduction occurs in a multi-stage mechanism involving bond breakage and reformation. Increase of the current density at higher anodic polarization potentials is corresponding to oxygen evolution reaction. No changes were observed after the 10^{th} cycle, allowing for the assumption about the stability of the investigated system. BDD surface progressively changes as a result of potential cycling,

showing increase of the anodic overpotential of oxygen evolution, in accordance with previous studies [29,33].

Exceeding the polarization level of +1.5 V vs $Ag|Ag_2SO_4$ is sufficient to initiate oxidation of hydrogen termination bonds on BDD and modify physic-chemical and electrochemical properties of the electrode**.** Under anodic polarization in acid media sp^2 graphite strongly corrodes and thus sp^2 impurities are removed producing CO and CO_2. It has been proved that removal of amorphous sp^2 carbon leads to increase in the working potential window as such impurities act as charge transfer mediators [19,20], explaining irreversible character of oxidation process. DFT simulations and experimental results run by Chaplin *et al*. [32] concluded that at potential values exceeding +1.8 V vs NHE carbon radicals are formed on the surface of BDD, that will further react without an activation barrier with OH radicals at potentials where water oxidation occurs.

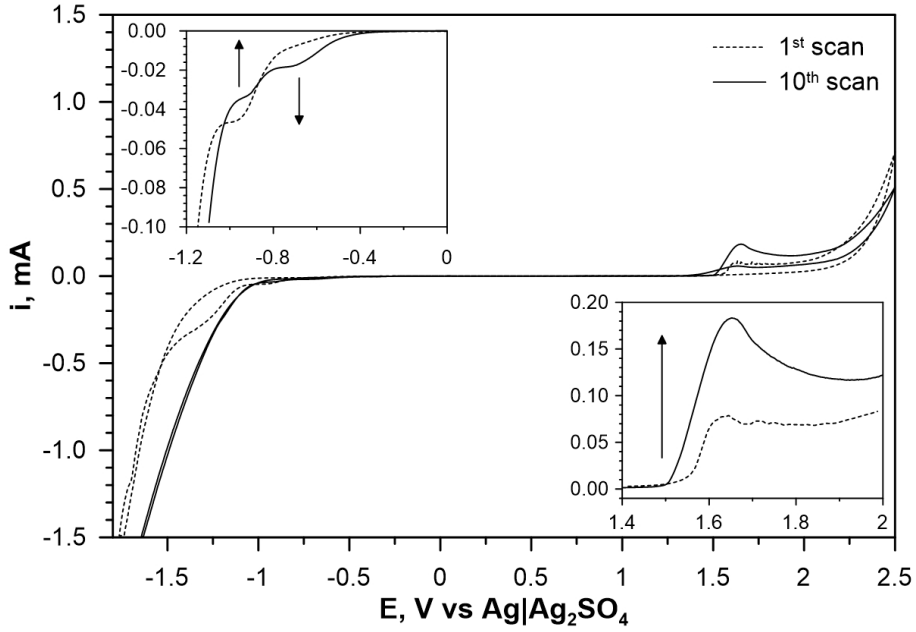

Fig. 2 – Typical cyclic voltammetry graph of BDD electrode, for the first scan (dashed line) and the tenth scan (solid line). In the bottom right inset, magnification of the anodic polarization sweep in range of oxidation of termination bonds, in the upper left inset, magnification of the cathodic polarization sweep in the range of hydrogen evolution. Polarization range -1.8 V to +2.5 V vs $Ag|Ag_2SO_4$. 1M H_2SO_4 solution. Polarization rate 1 mV/s.

Dynamic impedance spectra corresponding to changes of electrochemical properties as a result of anodic polarization were obtained using DEIS, applying predefined AC signal on

linear polarization sweep. Exemplary impedance data, in a form of Nyquist plot versus polarization potential, obtained for 10th polarization cycle, are presented on Fig 3a.

Dispersion of impedance spectra is visible at potentials close to the value of open circuit potential E_{OC}. In DEIS, excitation is performed continuously, and unlike for the classic approach, it is not possible to establish the proper current range for each subsequent spectrum. In this study, the value of current density changes by three decades during oxidation of termination bonds and the current range was chosen in a way to enable registration of the highest values of total DC and AC currents.

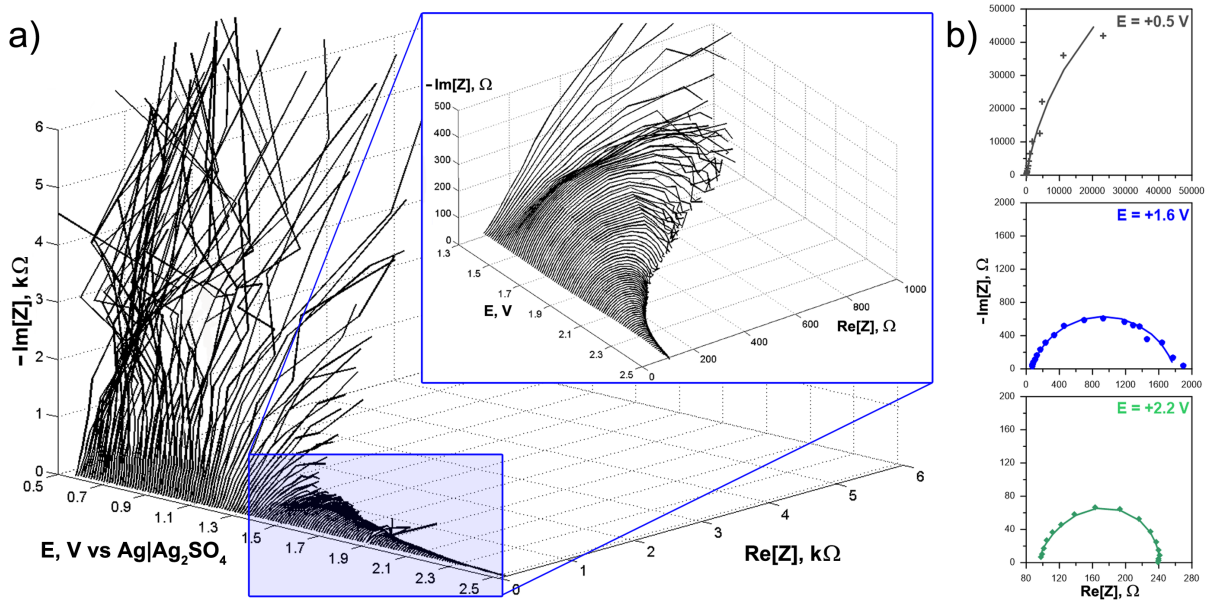

Fig. 3 – Impedance spectra in the form of Nyquist plot a) changes with potentiodynamic scan, in the inset magnification of the polarization range of oxidation of termination bonds; b) individual DEIS spectra at different anodic polarization potential with dots referring to experimental results and line show fitting to equivalent circuit R(C(R(QR))).

Acquisition of electric parameters requires fitting procedure and is carried out with the use of electric equivalent circuit. On its base, among others, charge transfer through the interface or depletion layer of semiconducting material are estimated. The equivalent circuit should include all the processes and interfaces and at the same time be simple enough to be physically explicable. Our previous results [33] show that an equivalent circuit $R_0(C_1(R_1(Q_2R_2)))$ consisting of two time constants was the most suitable choice, offering all above features, with reasonably small fitting error and monotonicity of data as a function of applied polarization potential. The two time constants, characterized by the impedance parameters (R_1, C_1) and (R_2, Q_2) were estimated for a high and low frequency range, respectively. The high-frequency time constant is contributed mostly by contamination of the

electrode surface with carbon having sp^2 hybridization. It is attributed to an irreversible process, since it stands out only during the first polarization scan and fades away with consecutive cycles. Similarly, the value of Q_2 parameter decrease by over an order of magnitude from the 1st to the 10th polarization cycle, which is presumably a result of removal of sp^2 contamination from the electrode surface. In the polarization range to +1.5 V vs $Ag|Ag_2SO_4$, R_1 resistance increases, as is often the case for limited amount of the reagent or diffusion control.

Resistance R_2 and capacitive parameter Q_2 at low frequency time constant for the 10th polarization cycle are shown on Fig. 4 and Fig. 5 respectively. R_2 is primarily associated with charge transfer resistance while the origin of Q_2 is more complex. Total differential double layer capacitance of a semiconductor surface C_{dl} is a sum of space-charge layer capacitance C_{cs}, the Helmhotz layer C_H and the diffuse layer capacitance C_d [29], while the smallest capacitance will dominate Q_2. In the low anodic polarization range, Mott-Schottky dependence reveals linear character resulting from p-type semiconductor. Space-charge capacitance is a determining factor, but once particular oxidation potential is reached Q_2 behavior is corresponding additionally to capacitance of a Helmhotz layer and diffuse layer forming on the interface between BDD and electrolyte.

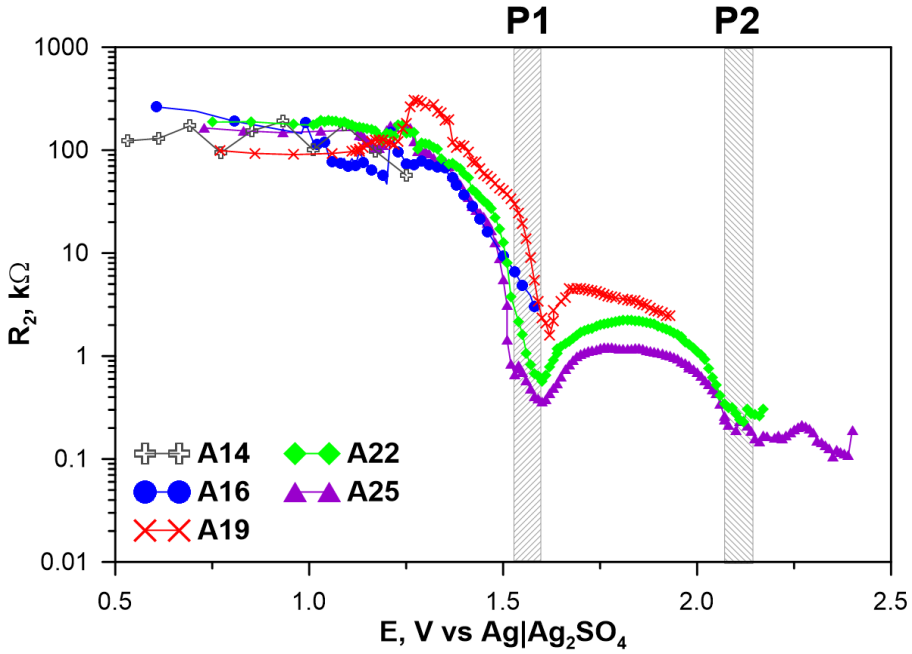

Fig 4 – Changes of R_2 describing the resistance of low frequency time constant according to equivalent circuit R(C(R(QR))). Samples subjected to potentiodynamic conditions with different anodic polarization limit between +1.4 V and +2.5 V vs $Ag|Ag_2SO_4$.

Fig. 4 illustrates that the electrochemical modification of BDD terminating bonds meaningfully affects charge transfer resistance, R_2. For each investigated sample, its value drops by over two orders of magnitude after reaching polarization +1.4 V vs $Ag|Ag_2SO_4$. Hydrogen terminated BDD electrode has a very high value of charge transfer resistance, reaching up to and exceeding 100 kΩ. For objects owing high values of impedance the limitation of excitation frequency range and acquisition time (size of analyzing window) in DEIS methodology introduce a significant error during the fitting procedure. Dispersion of results, recorded between each sample at low anodic polarization range comes additionally from problems with the current range selection, described earlier in the manuscript [39]. Between polarization potentials +1.4 V to +1.6 V vs $Ag|Ag_2SO_4$ R_2 drops under 0.5 kΩ, this is the first stage of the oxidation process: P1. A decrease of R_2 beyond +1.9 V vs $Ag|Ag_2SO_4$ results from further oxidation of the electrode (second stage: P2) and finally from oxygen evolution reaction at the electrode surface. The above-mentioned changes are apparent for each investigated sample, however measurement carried out at deeper oxidation potentials (A22 and A25) reveals improved development, allowing to draw a conclusion that polarization potential and/or time of exposure to oxidation conditions influence efficiency of the oxidation process. The deeper the polarization range, the lower the value of registered instantaneous charge transfer resistance as can be seen for polarization potentials above P1 on Fig. 4. This trend originates from different level of removal of sp^2 carbon impurities. The above study is in good agreement with EIS results for BDD obtained at different anodic charges [32]. Table 1 concludes the observation regarding dependence between polarization potential and oxidation degree.

Table 1.Samples subjected to electrochemical treatment in potentiodynamic conditions under different anodic polarization limits.

Name	Polarization range vs $Ag|Ag_2SO_4$		Oxidation phase
A05	-1.8 V	0.5 V	< P1
A14	-1.8 V	1.4 V	< P1
A16	-1.8 V	1.6 V	~ P1
A19	-1.8 V	1.9 V	< P2
A22	-1.8 V	2.2 V	~ P2
A25	-1.8 V	2.5 V	> P2

Prominent drop of charge transfer resistance exceeding the polarization potential of +1.4 V vs $Ag|Ag_2SO_4$ is preceded by an increase of capacitive parameter Q_2. Such a relationship is characteristic for relaxation processes [24] and occurs twice during the measurement; a subsequent drop of Q_2 is visible on exceeding polarization +2.0 V vs $Ag|Ag_2SO_4$, also leading to further decrease in R_2. Increase of capacitance value is caused by formation of a diffuse layer and adsorption of reagents. This layer is absent at lower polarization potentials explaining weak interactions of diamond with ionic or dissolved species [20,29,40]. An electrochemical reaction, that follows at higher polarization potentials leads to a decrease of thickness of layer and thus decrease of capacitive parameter. An aggregate increase of capacitance with applied charge may be also related to the electrochemical removal of non-diamond phases at the grain boundaries increasing the surface area and the density of charged sites at the electrode surface [41].

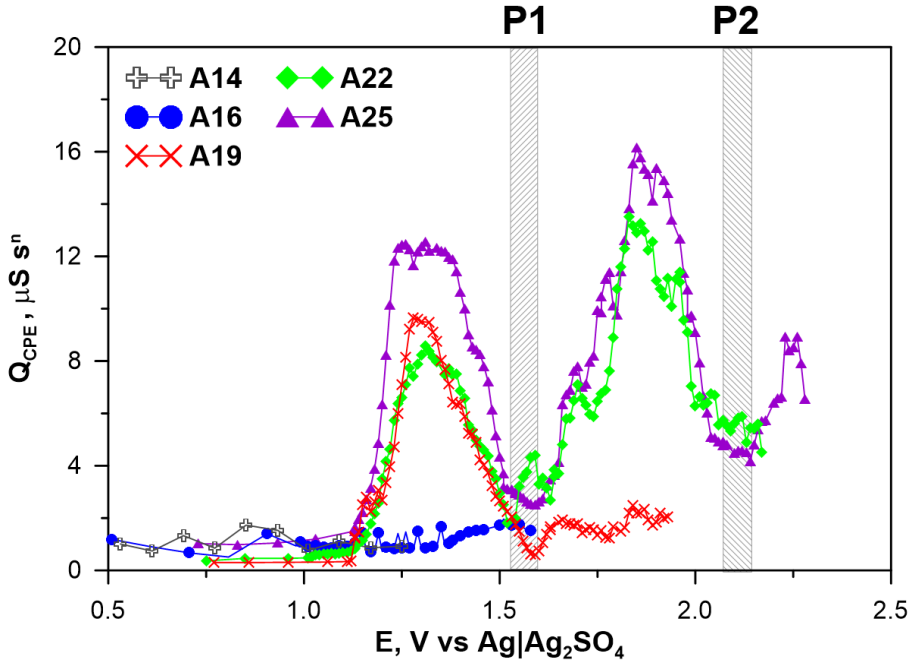

Fig 5 – Changes of constant phase element Q_2, used to describe the capacitive parameter of low frequency time constant according to equivalent circuit R(C(R(QR))). Samples subjected to potentiodynamic conditions with different anodic polarization limit between +1.4 V and +2.5 V vs $Ag|Ag_2SO_4$.

An odd dependence was found for Q_2 behavior around P1 transition of sample polarized to +1.6 V and similar for P2 transition of sample polarized to +1.9 V vs $Ag|Ag_2SO_4$. Capacitive parameter alteration as a function of potential show a flat line, with no peaks present. Anodic polarization range set-up in these measurements was not sufficient to initiate electrochemical

reaction (as can be concluded from position of R_2=$f_{(E)}$ local minimum on Fig. 4). In order to initiate the oxidation process, a sample must earlier be subjected to anodic polarization beyond a certain potential range. These results confirmed that the removal of sp^2 carbon impurities and activation of radical play an important role in the oxidation process of termination bonds on BDD electrode.

Anodic polarization affects the purity of the electrode surface. Once sp^2 carbon is removed, the formation of oxygenated carbon groups under anodic polarization exceeding the flat-band potential lead to increase of electronic surface states density, deviating the BDD electrode behavior from p-type semiconductor [42]. It should be noted (and will be further discussed), that according to Pleskov *et al.* [43] (110) and (111)-orientated BDD grains possess more positive value of flat-band potential than (100)-orientated grains. E_{fb} shift ranging up to +0.7 V is in good agreement with observed potential gap between initiation of oxidation processes P1 and P2.

3.2 Physic-chemical surface analysis

After completion of 10^{th} anodic polarization cycle samples were removed from electrolyte, washed and undergone XPS examination to compare differences in surface oxidation after reaching certain anodic potential. High-resolution C1s spectra of samples, previously subjected to different anodic polarization levels, are presented on Fig. 6a. It can be observed that as a result of anodic polarization peak shifts towards more positive values of binding energy (BE), but only after exceeding the potential of P1 process initiation (>1.6 V vs $Ag|Ag_2SO_4$) the shape of the peak undergoes a significant change.

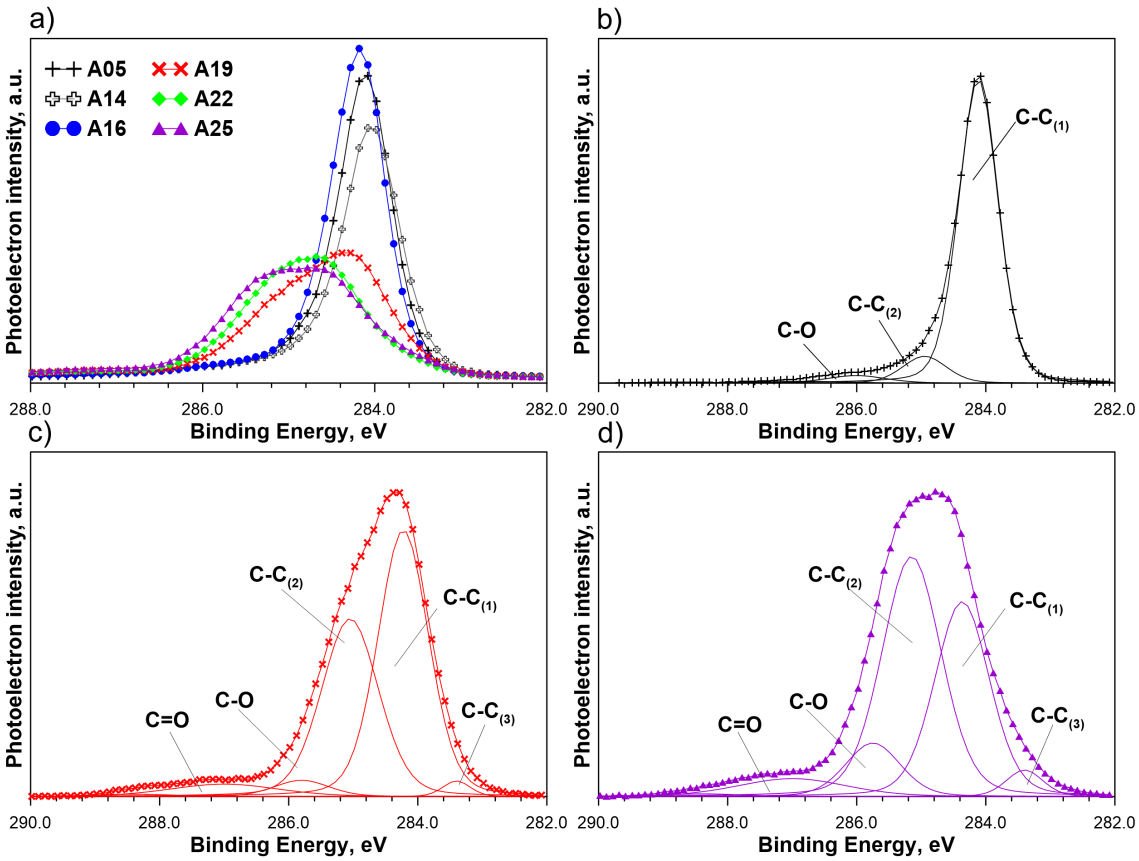

Fig. 6 – High resolution XPS spectra recorded for carbon region C1s for BDD samples at different levels of anodic oxidation; a) overview; b-d) as a result of 10 consecutive scans in the range of potentials between -1.8 V and +0.5, +1.6, +2.5 V respectively.

XPS C1s spectrum of hydrogen terminated BDD samples A05 and A14 (Fig. 6b) reveals two main peak components, C-$C_{(1)}$ located at approx. 284.2 ± 0.1 eV and C-$C_{(2)}$ shifted by +0.8 eV. According to Ballutaud *et al.* [44] those peaks correspond to hydrogenated and non-hydrogenated diamond surface, respectively. The last component, shifted by +1.6 eV may be attributed to C-O ether bonds. The relative concentration of oxygen on the surface reaches ~7% and originates from storing BDD electrodes in air conditions. All of those results are in good agreement with previous findings [3,5,34,44-46].

As a result of anodic oxidation beyond P1 (Fig. 6c-d), the contribution of C-$C_{(2)}$ and C-O peaks greatly increase, simultaneously limiting the area under C-$C_{(1)}$ peak. A wide tail present at more positive values of BE indicates the necessity of addition of new deconvolution peaks shifted by +2.7 eV even up to + 4.1 eV in respect to C-$C_{(1)}$. These peaks, collectively identified as C=O, are attributed to carboxyl, carbonyl and ether bonds. The amount of analyzed oxygen raised even up to ~14.5%.

Prolonged anodic oxidation of BDD electrode leads to the appearance of another phase of carbon, represented on C1s spectrum by peak C-$C_{(3)}$, located around 283.4 eV. This component is usually ascribed to the sp^2 carbon (C=C) at the diamond surface [46], however its contribution in overall spectrum is increasing over time and as such does not agree with impedance measurements and previous reports. Ghodbane *et al.* [21] observed a similar effect for polycrystalline electrodes and attributed this component to the presence of surface dimers. Polcaro *et al.* [22] suggest that the presence of distorted diamond can be related to the vacancies of hydrogen atoms close to boron atoms, as a result of oxidation of termination bonds. B atoms are included in the lattice as sp^2 terminations and the presence of hydrogen atoms brings the valence to sp^3. At the same time, an increase of free H atoms in the lattice can form trans-polyacetylene segments at the grain boundaries [47]. Such phenomena can become a significant factor as a result of ageing, leading to formation of a graphitic phase at the grain boundaries and accelerating degradation of diamond crystals [48].

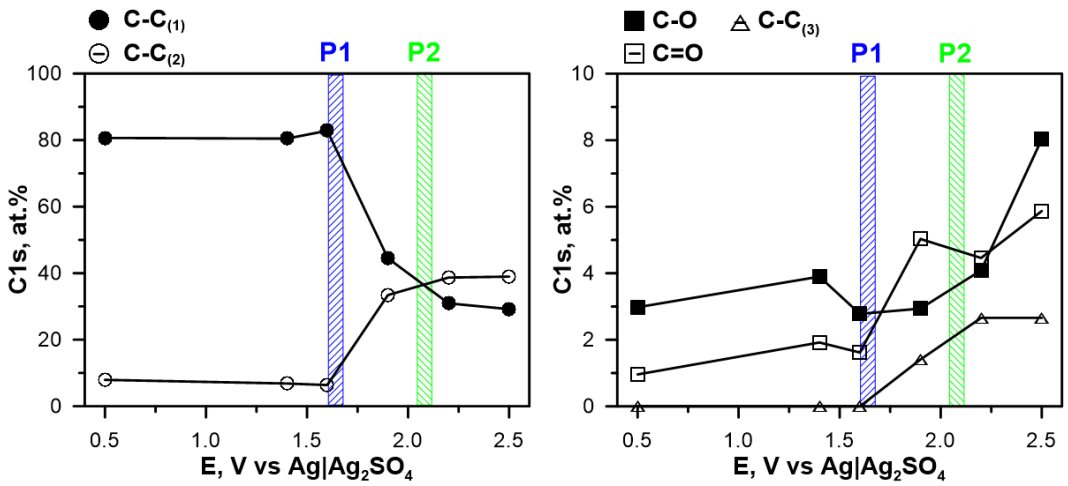

Fig. 7 – Influence on anodic polarization level on the percentage contribution of each component in high resolution XPS analysis of C1s, calculations include oxygen.

The degree of hydrogen termination at the surface of BDD rapidly decreases as a result of polarization beyond potential +1.6 V vs $Ag|Ag_2SO_4$ (exceeding P1), this change is accompanied by an increase of contribution of oxygen terminated BDD, as seen on Fig. 7 and in Table 2. At the same time, the amount of carbon-oxygen bonds increase as well. Irreversible degradation of BDD electrode, taking place only as a result of oxidation of termination bonds can be tracked by means of C-$C_{(3)}$ peak share.

Table 2 – Percentage contribution (at.%) of carbon after deconvolution of C1s peak and oxygen on the base of high-resolution XPS analysis.

Name	$C\text{-}C_{(1)}$ 284.2 eV	$C\text{-}C_{(2)}$ 285.0 eV	$C\text{-}C_{(3)}$ 283.4 eV	C-O 285.9 eV	C=O 287.0 eV*	O-C 531.1 eV^{+}
A05	80.6	7.9	--	3.0	1.0	7.5
A14	80.4	6.8	--	3.9	1.9	6.9
A16	82.8	6.4	--	2.8	1.6	6.4
A19	44.5	33.4	1.4	2.9	5.0	12.7
A22	30.9	38.7	2.7	4.1	4.5	19.2
A25	29.2	37.0	2.7	8.0	5.9	17.3

* The percentage composition of carbon marked as C=O is a sum of two peaks, located at 287.0 eV for carbonyl bonds and 288.4 eV for carboxyl bonds. $^{+}$ The percentage composition of oxygen marked as O-C is a sum of two peaks, located at 531.1 eV for C-O and located at 532.0 eV for C=O bonds.

3.3. Oxidation of termination bonds

We suggest that there are three main reasons responsible for multistage mechanism of oxidation of termination bonds on BDD polycrystalline electrode, as can be seen in Fig. 8. Those reasons are: (A) different types of termination are initiated with certain anodic polarization level; (B) heterogeneity of boron incorporation or (C) crystallographic orientation leads to different polarization potentials required for oxidation of termination bonds.

It may be that above the threshold of +1.5 V vs $Ag|Ag_2SO_4$ (i) certain anodic polarization potential or (ii) certain oxidation time influences the type of oxidation. Initially, the electrode surface is oxidized and becomes terminated with hydroxyl groups (A). Termination with carbonyl or ether bonds requires higher anodic potentials/oxidation time. This hypothesis is in good agreement with XPS results. The significant drop of hydrogenated diamond surface has been observed exceeding polarization of 1.5 V (exceeding P1), yet the amount of C-O bonds increase more rapidly beyond 2.1 V vs $Ag|Ag_2SO_4$ (exceeding P2). Further, the oxidation levels may be initiated by time of oxidation. A similar conclusion was delivered out by Ghodbane *et al.* [18] as a result of HREELS analysis of nanocrystalline diamond films. Those results conclude initial insubstantial traces of OH functions, transformed into ether or carbonyl groups as the oxidation process continues. Wang *et al*. [5] observed that through longer oxidation times C-O-C groups are preferentially formed, as linked to a severe reconstruction of the diamond surface.

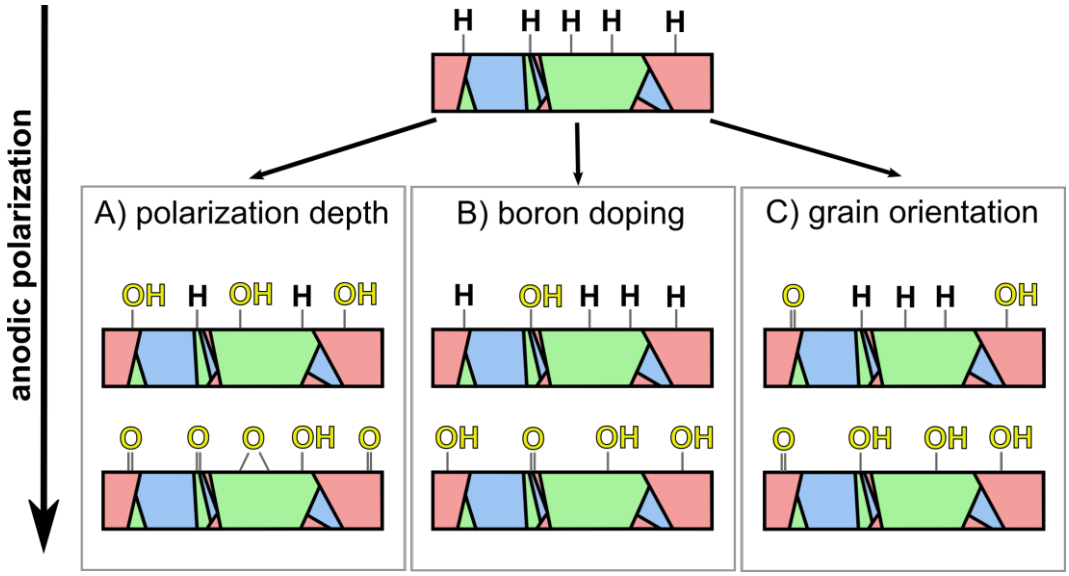

Fig 8 – A schematic representation of different initiators of heterogeneous oxidation process of BDD termination bonds under anodic polarization conditions: a) formation of different types of bonds activated under different polarization level; b) influence of higher boron doping at grain boundaries; c) effect of electrochemical activity of crystallographic orientation

In accordance with second reason (B) local heterogeneities of boron doping or sp^2 carbon removal should be considered. Boron atoms either substitute carbon atoms or accumulates at the grain boundaries [49,50], simultaneously leading to different sp^3/sp^2 ratio. The higher the doping level, the lower the grain size [28], and for heavily doped electrodes grain boundaries cover substantial area of the electrode. Carbon atoms located at such heavy doped grain boundaries might be oxidized at lower polarization potentials. Ghodbane *et al.* [21] proved that increase in boron doping level from $4x10^{20}$ cm^{-3} to $2x10^{21}$ cm^{-3} influence location of C1s peak on XPS results, shifting it by over -1.0 eV. In this case peak marked as $C\text{-}C_{(2)}$ on Fig. 6b-d would also correspond to C-O bonds at the grain boundaries.

The third option (C) is linked to the different oxidation degrees of grains due to different crystallographic orientation. An impact of crystallographic orientation on local electrochemical properties of the sample (such as corrosion susceptibility of metals) is in spotlight of scientists in many fields [52]. It is known that BDD electrodes of different crystallographic orientation affects the boron uptake and originates from different boron incorporation from the feeding gas to different diamond crystal faces during their growth. According to Pleskov *et al.* [52] the lowest acceptor (boron) concentration is present in (100)-orientated faces, while the electrode behaviour of (111)-orientated face approaches that of metal-like electrodes. The value of flat-band potential E_{fb}, obtained by means of Mott-Schottky analysis, is higher for (110) and (111)-orientation than (100) by approx.

+0.3 V and +0.7 V, respectively [43]. The positive value of E_{fb} is explained by the oxidized state of the diamond surface. These findings are in agreement with both (B) and (C) hypothesis. It was also observed that the oxidation/reduction process of $[Fe(CN)_6]^{3-/4-}$ is more likely to proceed for (110) and (111)-orientated grains. Against, for (100) orientation proceed under kinetic, rather than diffusion, control due to higher resistivity. These findings are in good agreement with AFM study of polycrystalline OT-BDD electrodes carried by Hoffmann *et al.* [6], revealing nanoscale heterogeneities of the oxidation level.

Most likely, all of the above-mentioned variables have some influence on the outcome of oxidation of termination bonds. Wilson *et al.* [53] and Zielinski *et al.* [49] carried out AFM and SECM investigation and concluded that boron uptake is non-uniform across the surface of OT-BDD, by locating the variations of conductivity that correspond to geometry of individual grains. Different levels of boron incorporation may, however, be connected with crystallographic orientation.

3.4. Reversibility of oxidation process

To verify the reversibility of the oxidation process taking place on BDD electrode surface under the presence of electrochemical factor, we conducted an additional experiment in potentiodynamic conditions, performing a single CV measurement (polarization rate 1 mV/s) vs different polarization depths. The first set of samples was polarized to +1.6 V vs $Ag|Ag_2SO_4$ (BA16) and +2.5 V vs $Ag|Ag_2SO_4$ (BA25) assuring the presence of transformed OT-BDD. In the next set, samples were polarized up to +2.5 V vs $Ag|Ag_2SO_4$, followed by a cathodic scan beyond potential of hydrogen evolution. Then, one sample was removed from the electrolyte immediately (BC18), while the latter was kept at -1.8 V vs $Ag|Ag_2SO_4$ for another 100 seconds (BC181). These results were compared with the reference samples B0 (no polarization) and BA10 (anodic polarization in the range of potentials not exceeding oxidation process). Detailed experimental conditions are presented in Table 3.

Oxidation degree and reversibility of the process were investigated on-line by means of CV and DEIS techniques and assisted off-line with wettability angle investigation and spectroscopic ellipsometry. These techniques are surface sensitive, however unlike XPS they are not highly influenced by the adsorbed layer formed as a result of keeping samples in air conditions. Ostovskaya el al. [54] investigated wettability of oxygen and hydrogen plasma-treated diamond films. Those authors show that hydrogen plasma treatment can change the

bond from C(1 × 1) to C(2 × 1):H reconstruction to form C-C surface dimers. Moreover, the C-C bond length changes due to plasma-treatment and becomes similar to graphite. Hence, there is appearance of the highly oriented sp^2 on the surface or between crystallites. On the other hand, the atomic oxygen can reduce C(2 × 1) to C(1 × 1) even in room temperature forming oxygen layers, which is favorable for the (100) plane.

Wettability angle measurements are listed in Table 3. It can be seen, that both samples: B0 and BA10 are characterized by a similar wetting, close to 70 degrees, while measurements on the B0 sample are characterized by much smaller standard deviation of results, which is most likely due to not being exposed to electrolytic conditions. Wettability angle of BA25 sample diminished by over 25 degrees, its hydrophilicity increase results from oxygen-terminated BDD surface. Hydrogenation process under cathodic polarization results in an increase of wettability angle, reaching values similar to BA16 sample. Nevertheless, hydrogenation seems to be only partial if the electrode is polarized under deep cathodic potentials for extended periods of time.

Table 3 - Samples subjected to electrochemical treatment in potentiodynamic conditions to investigate on the reversibility of the oxidation process.

Name	Polarization limit	Measurement finish at	Wettability angle	Type of termination
B0	-	-	70.1 ± 0.9	HT-BDD
BA10	+1.0 V	+1.0 V	73.0 ± 1.7	HT-BDD
BA16	+1.6 V	+1.6 V	50.2 ± 1.9	OT-BDD
BA25	+2.5 V	+2.5 V	45.0 ± 2.0	OT-BDD
BC18	+2.5 V	-1.8 V	53.2 ± 3.5	Partial
BC181	+2.5 V	-1.8 V *	56.4 ± 4.0	Partial

* The experiment was extended by a potentiostatic polarization for a period of 100s at potential -1.8 V. All potentials presented in table 3 were obtained vs $Ag|Ag_2SO_4$ reference electrode.

Ellipsometry found a wide application range for investigating of very thin films and surface processes, due to very high measurement sensitivity. However, no detailed conclusions can be drawn without performing fitting procedure, which is very complex in the case of polycrystalline samples. It was observed that in a wide range of wavelengths spectra of oxidized samples behave differently from hydrogenated ones. As presented in Figure 9, the variation of Delta as a function of photon energy is steeper for HT-BDD (a decrease of 6 degrees). The oxidized BDD sample shows Delta decrease by a value of 2 degrees, while

the longer the exposition time to cathodic conditions, the lower Delta drop (down to 6 for BC181).

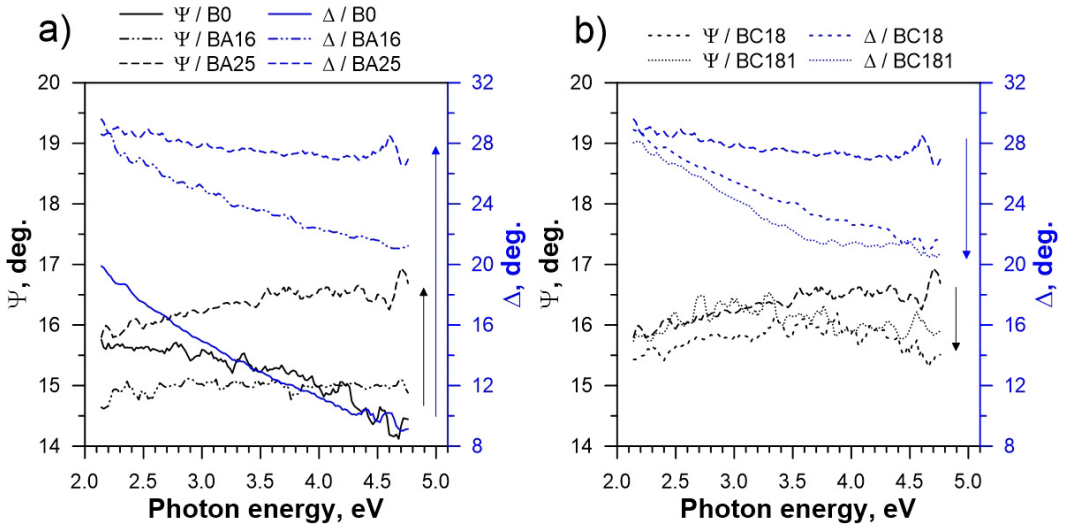

Fig. 9 – Spectral variation of Delta and Psi ellipsometric angles for investigated conditions: a) samples BA16 and BA25 compared to reference HT-BDD B0; b) effect of cathodic reduction for samples BC18 and BC181.

By fitting the experimental and theoretical ellipsometric spectra over a wide wavelength range, the effective dielectric function of the BDD electrode can be determined (see Figure 10). The SE results could be directly compared with other techniques measuring surface properties such as CV or DEIS measurements since SE measures the dielectric constants.

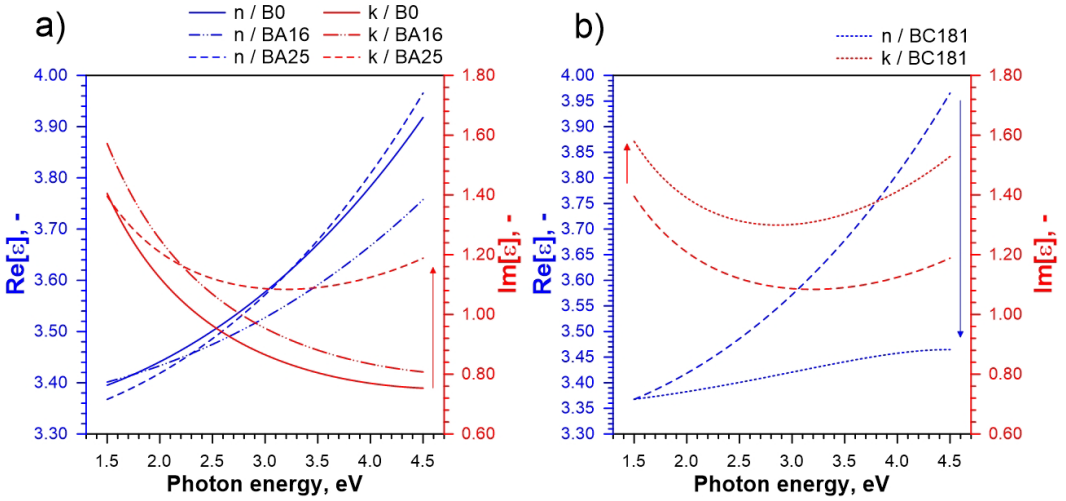

Fig. 10 – Spectral variation of optical constants for boron-doped diamond films. a) samples BA16 and BA25 compared to reference HT-BDD B0; b) effect of cathodic reduction for sample BC181.

The shape of the effective dielectric function of the B-NCD films in the IR photon energy range was modelled using the Drude term. The B16 electrode shows that the dielectric constants are just slightly increased comparing to the B0 one. This comes from the partial oxidation of the electrode. Nevertheless, the Epsilon(Im) rises, with increases in potential range up to +2.5 V vs $Ag|Ag_2SO_4$, from 0.8 to 1.2 at 260 nm (4.5 eV) comparing with electrode B0 or BA16 to BA25 (Fig. 10a). This fact is in agreement with our former results [27] showing a similar trend with increase in the B concentration in the films. It suggests that full oxidation was achieved and more boron atoms at the electrode surface are activated becoming acceptors in the electrochemical system. It could be concluded that the additional semiconductor-metal transition was reached.

Moreover, several reasons could be the explanation of this phenomenon. The most possible are as follows: (I) overpotential cathodic treatment causes deep sp^2 phase removal covering active boron clusters or interstitial B incorporation, which does not contribute to generate free holes [6,49] or (II) high overpotentials modifies the structure of the electrode affecting in distorted Fermi surface, which results in excess carrier concentration [55].

The influence of boron concentration in NCD films were studied elipsometrically by Zimmer *et al.* [56], who applied the Lorentzian oscillator to describe the IR absorption of the B-NCD films. The energy of the absorption line found in their investigation ranged from 0.09 eV to 0.29 eV depending on the layer thickness and the shape of the absorption line (Lorentz or Tauc-Lorentz oscillator) used to characterize the UV features of the dielectric response of these films. This energy value is close to the boron acceptor level (0.38 eV) [57,58].

Analyzing the dielectric constants of the cathodic treated electrode BC161 illustrated in Figure 10b, we can conclude that Epsilon(Re) becoming significantly weaker and Epsilon(Im) increases of 0.2. This strongly suggests that the electrode becomes degraded including transformation to some sp^2 phases like carbon dimers [21] or trans-polyacetylene groups [47] as concluded in previous subsections.

Figure 11 shows a change of instantaneous impedance spectra as a result of reverse polarization for sample BC18. It can be observed that application of polarization below value of E_{OC} significantly modifies the spectra, here presented in the form of Nyquist plot. An initial decrease of the semicircle is connected to drop of polarization resistance, proportionally to cathodic polarization level. This relationship is linear within the potential range between E_{OC}

and -0.6 V vs $Ag|Ag_2SO_4$. Exceeding the polarization potential of -0.6 V leads to the appearance of low frequency inductive loop, which then disappears below the potential -1.10 V vs $Ag|Ag_2SO_4$ and is reformed into loop with positive capacitance values. The above-described phenomenon is typical for hydrogen evolution reaction, according to Volmer-Heyrovsky model [59]. The process of hydrogen evolution consists of two reactions; in the first step a hydrogen species is adsorbed on the electrode surface from the solution and in the second step two adsorbed hydrogen ions electrochemically desorb to form hydrogen particle. The total rate of the process is always determined by the rate of the slower of two reactions and is a function of applied polarization level.

If the reaction rate of adsorption of hydrogen atoms is higher than the reaction rate of their desorption and formation of H_2, then the electrode surface becomes covered with the adsorption layer, as is in the case of potentials between -0.60 V and -1.10 V vs $Ag|Ag_2SO_4$. It is worth noting that in this potential range a small increase of cathodic currents can be seen on CV diagram presented in Fig. 2. The current density associated with this region increases with consecutive polarization sweeps, suggesting that higher surface area is activated for adsorption of hydrogen from the electrolyte. This behavior is most likely connected to the irreversible reduction of the sp^2 carbon and increase of the electrode area. Beyond the potential of -1.10 V vs $Ag|Ag_2SO_4$, the rate of desorption process exceeds the rate of the adsorption process thus leading to removal of the adsorption layer from the electrode surface and the hydrogen evolution reaction is now controlled by the adsorption rate. Cathodic currents increase exponentially according to Butler-Volmer formula [59].

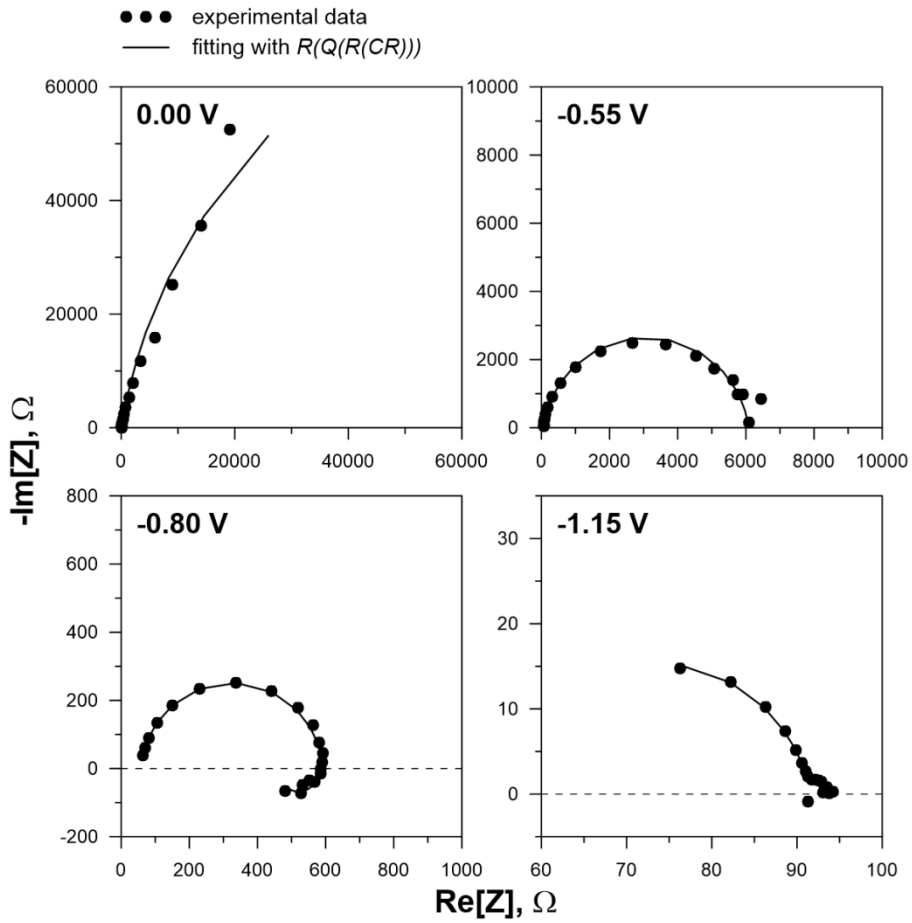

Fig 11 – Exemplary instantaneous impedance spectra in the form of Nyquist plot obtained by DEIS technique under cathodic polarization sweep for sample BC18. Dots refer to experimental results and line show fitting with equivalent circuit R(QR) for spectra acquired at potentials 0.00 V and -0.55 V vs Ag|Ag_2SO_4 and R(Q(R(CR))) for remaining spectra (-0.80 V and -1.15 V vs Ag|Ag_2SO_4).

The selection of electric equivalent circuit assuring its proper physical interpretation is very complex, especially in the range of hydrogen evolution, where additional time constant must be included for fitting of data in low frequency range. Although, it was not the initial goal of our study, we have decided to select one and perform the preliminary fitting procedure. Moreover, an equivalent circuit must include the appearance of the inductive loop. In the study on interpretation of impedance comprising negative capacitance Elkin *et al.* [60] drew a conclusion that inductance cannot be associated with accumulation of energy in the magnetic field at the solid electrode surface and suggested the use of negative capacitance instead of inductance for interpretation of the adsorption faradaic systems. Elkin also suggests that the negative capacitance is the consequence of the interaction of two consecutive flows that form a two-stage faradaic process of intermediate adsorption. On the other hand, the use of R_1C_1 time constant connected with sp^2 carbon impurities, applied in previous examination becomes

obsolete after removal of those impurities. For this reason, an electric equivalent circuit $R_0(Q_2(R_2(C_3R_3)))$ was proposed, where C_3R_3 are ascribed to the adsorption layer.

Changes in value of electric parameters revealed linear decrease of R_2 with cathodic polarization, therefore suggesting a dominant role of polarization resistance. No local minimum was observed, which confirms lack of relaxation process in range of potentials prior to hydrogen evolution. Likewise, the value Q_2 remains constant.

Table 4 – Electric parameters calculated on the base of R(Q(R(CR))) equivalent circuit under different levels of cathodic polarization.

Cathodic polarization potential vs $Ag\|Ag_2SO_4$	R_2 kΩ	Q_2 μSs^n	n -	R_3 Ω	C_3 μF
0.00 V	187.90	4.15	0.89	--	--
-0.55 V	6.02	1.67	0.92	--	--
-0.80 V	0.53	1.32	0.96	-140	-910
-1.15 V	0.04	2.39	0.89	2	1570

Finally, to define the level of reversibility in the area of cathodic polarization corresponding to hydrogen adsorption layer formation and corresponding to hydrogen particle formation according to Volmer-Heyrovsky mechanism XPS study was performed. Two electrodes were initially polarized anodically, the same way as A25 sample and afterwards kept at potential of -0.85 V and -1.20 V vs $Ag|Ag_2SO_4$ for a period of 20 minutes. Results of deconvolution of high-resolution C1s and O1s peaks are listed in Table 5, done on the base of the same fitting procedure as presented earlier in the manuscript.

Table 5 - Percentage contribution (at.%) of carbon after deconvolution of C1s peak, oxygen and sulphur on the base of high-resolution XPS analysis.

Cathodic polarization potential vs $Ag\|Ag_2SO_4$	$C\text{-}C_{(1)}$ 284.2 eV	$C\text{-}C_{(2)}$ 285.0 eV	$C\text{-}C_{(3)}$ 283.4 eV	C-O 285.9 eV	C=O 287.0 eV	O-C 531.1 eV	S 168.3 eV
-0.85 V	47.2	34.6	0.5	5.1	3.3	6.4	0.4
-1.20 V	35.4	25.0	0.7	4.5	3.2	5.9	5.8

Contrary to earlier studies, sulphur S2p peak doublet was observed for both of the samples. Its share in total concentration was 0.4% and 5.8% for BC08 and BC12, respectively. The position of $S2p_{3/2}$ peak was 168.3 eV, which corresponds for BE of sulphates [61]. On the

other hand, no peak was observed for BE of 163.8 eV, typical for C-S bond, such as for DMS [62]. These results allow us to draw a conclusion about contamination of electrode surface with a thin layer of sulphates. The ratio $C\text{-}C_{(1)}/C\text{-}C_{(2)}$, equals to 1.36 for BC08 and 1.41 for BC12, which is a similar result to A19 sample showing 1.33 ratio. Concentration of $C\text{-}C_{(1)}$ and $C\text{-}C_{(2)}$ indicates that the reversibility of the electrode is not complete, thus confirming earlier wettability angle and ellipsometric studies. An important observation concerns the amount of sulphur present at the electrode surface, it drastically increases as a result of transition below reduction potential of SO_4^{2-} to SO_3^{2-} at -1.20 V vs $Ag|Ag_2SO_4$ (-0.93 V vs NHE). It is evident that exceeding cathodic polarization beyond the value of potentials responsible for hydrogen evolution does not improve the reversibility while leading at the same time to contamination of the electrode with sulphuric compounds.

4. Conclusions

We have performed a deep study of the phenomena of oxidation of BDD termination bonds and concluded that the process occurs in a complex way, under three determining factors, being anodic oxidation level, boron incorporation and crystallographic orientation. These factors decide about the rate and homogeneity of the OT-BDD coverage. On the basis of DEIS and XPS study, it is evident that the most important factor influencing oxidation process is value of anodic polarization potential. The highest drop of electric parameters was observed exceeding potential of +1.5 V vs $Ag|Ag_2SO_4$, however a second indisputable transition occurs above +2.1 V vs $Ag|Ag_2SO_4$. A different oxidation degree of carbon on the surface of BDD electrode was present, depending on the anodic potential applied.

Changes of electric parameters in the function of polarization potential, obtained by means of DEIS technique allows to confirm earlier theoretical studies on the oxidation of termination bonds from HT- to OT-BDD. Our study reveals that HT- to OT- could undergo only if sp^2 contamination is removed from the electrode surface, after which the oxidation of termination bonds proceeds at anodic potentials above E_{fb} value.

According to the theory of Hoffmann *et al.* presented earlier [23], the electrode potential of -3.68 V vs NHE is required for reduction of OT-BDD to HT-BDD. On the other hand, the earlier study of Chaplin *et al.* [31] reports partial reversibility of the electrode at much less negative potentials (-1.9 V vs NHE), accompanied by Volmer discharge reaction. In practice even smaller negative potential is sufficient to acquire partial reversibility.

Wettability angle measurement study suggests a possible partial reversibility of the oxidation of termination bonds obtaining secondary HT-BDD. Its mechanism is attributed with adsorption of hydrogen in the potential range of hydrogen evolution. Despite a possibility of such behavior, DEIS and ellipsometric results show that the hydrogenation of BDD surface cannot be reached due to several factors. The most important one is the irreversible character of removal of sp^2 contamination during the preceding oxidation process. XPS results confirmed that anodic oxidation to =C=O is irreversible even at deep reduction potentials and its formation can contribute to the ageing of the electrodes. Additionally, under cathodic polarization conditions reduction of sulphuric acid occurs, contaminating BDD electrode.

Reversibility of the process at less negative polarization potentials can, like oxidation, be explained by a multistage process, initiated at different conditions for different grains. A full reversibility of the electrode however, seems impossible due to the unrecoverable corrosion of graphite during anodic oxidation.

References

[1] Simon N, Girard H, Ballutaud D, Ghodbane S, Deneuville A, Herlem M, et al. Effect of H and O termination on the charge transfer of moderately boron doped diamond electrodes. Diam Relat Mater 2005;14(3-7):1179-82. doi:10.1016/j.diamond.2004.12.013

[2] Yagi I, Notsu H, Kondo T, Tryk DA, Fujishima A. Electrochemical selectivity for redox systems at oxygen-terminated diamond electrodes. J Electroanal Chem 1999;473(1-2):173-8. doi:10.1016/S0022-0728(99)00027-3

[3] Denisenko A, Pietzka C, Romanyuk A, El-Hajj H, Kohn E. The electronic surface barrier of boron-doped diamond by anodic oxidation. J Appl Phys 2008;103:014904. http://dx.doi.org/10.1063/1.2827481

[4] Boukherroub R, Wallart X, Szunerits S, Marcus B, Bouvier P, Mermoux. Photochemical oxidation of hydrogen boron-doped diamond surface. Electrochem Commun 2005;7(9):937-40. doi:10.1016/j.elecom.2005.05.010

[5] Wang M, Simon N, Decorse-Pascanut C, Bouttemy M, Etcheberry A, Li M, et al. Comparison of the chemical composition of boron-doped diamond surface upon different oxidation processes. Electrochim Acta 2009;54(24):5814-24. doi:10.1016/j.electacta.2009.05.037

[6] Hoffmann R, Obloh H, Tokuda N, Yang N, Nebel CE.Fractional Surface Termination of Diamond by Electrochemical Oxidation. Langmuir 2012;28(1):47-50. DOI: 10.1021/la2039366

[7] Szunerits S, Boukherroub R. Different strategies for functionalization of diamond surface. J Solid State Electr 2008;12(10):1205-18. doi:10.1007/s10008-007-0473-3

[8] Zou YS, He LL, Zhang YC, Li ZX Wang HP, Gu L, et al. Construction and surface enhanced Raman scattering activity of gold nanoparticles array on boron doped diamond film. Mater Chem Phys 2013;141(2-3):816-21 doi:10.1016/j.matchemphys.2013.06.009

[9] Remes Z, Choukourov A, Stuchlik J, Potmesil J, Vanecek M. Nanocrystalline diamond surface functionalization in radio frequency plasma. Diam Relat Mater 2005;15(4-8):745-48. doi:10.1016/j.diamond.2005.10.043

[10] Notsu H, Tatsuma T, Fujishima A. Tyrosinase-modified boron-doped diamond electrodes for the determination of phenol derivatives. J Electroanal Chem 2002;523(1-2):86-92. doi:10.1016/S0022-0728(02)00733-7

[11] Yang W, Auciello O, Butler JE, Cai W, Carlisle JA, Gerbi JE et al. DNA-modified Nanocrystalline diamond thin-films as stable, biologically active substrates. Nat Mater 2002;1:253-7. doi:10.1038/nmat779

[12] Nebel CE, Yang N, Uetsuka H, Osawa E, Tokuda N, Williams O. Diamond nano-wires, a new approach towards next generation electrochemical gene sensor platforms. Diam Relat Mater 2008;18(5-8):910-7. doi:10.1016/j.diamond.2008.11.024

[13] Gu H, Su X, Loh KP. Conductive polymer-modified boron-doped diamond for DNA hybridization analysis. Chem Phys Lett 2004;388(4-6):483-7. doi:10.1016/j.cplett.2004.03.046

[14] Bogdanowicz R, Sawczak M, Niedzialkowski P, Zieba P, Finke B, Ryl J. et al. Direct amination of boron-doped diamond by plasma polymerized allylamine film. Phys Status Solidi A 2014;211(10):2319-27. DOI: 10.1002/pssa.201431242

[15] Brillas E, Martinez-Huitle CA. Synthetic diamond films: preparation, electrochemistry, characterization and applications. Wiley. 2011.

[16] Baldan MR, Azevedo AF, Couto AB, Ferreira NG. Cathodic and anodic pre-treatment boron doped diamond with different sp^2 content: Morphological, structural, and impedance spectroscopy characterizations. J Phys Chem Solids 2013;74(12):1830-5. doi:10.1016/j.jpcs.2013.07.015

[17] Medeiros de Araujo D, Canizares P, Martinez-Huitle CA, Rodrigo MA. Electrochemical conversion/combustion of a model organic pollutant on BDD anode: Role of sp^3/sp^2 ratio. Electrochem Commun 2014;47:37-40. doi:10.1016/j.elecom.2014.07.017

[18] Ghodbane S, Haensel T, Coffinier Y, Szunerits S, Steinmuller-Nethl D, Boukherroub R, et al. HREELS investigation of the surface of nanocrystalline diamond films oxidized by different processes. Langmuir 2010;26(24):18798-805. DOI: 10.1021/la1032652

[19] Duo I, Fujishima A, Comninellis Ch. Electron transfer kinetics on composite diamond (sp^3)-graphite(sp^2) electrodes. Electrochem Commun 2003;5(8):695-700. doi:10.1016/S1388-2481(03)00169-3

[20] Swain GM. The susceptibility to surface corrosion in acidic media: a comparison of diamond, HOPG, and glassy carbon electrodes. J Electrochem Soc 1994;141(12):3382-93. doi: 10.1149/1.2059343

[21] Ghodbane S, Ballutaud D, Omnes F, Agnes C. Comparison of the XPS spectra from homoepitaxial{111}, {100} and polycrystalline boron-doped diamond films. Diam Relat Mater 2010;19(5-6):630-6. doi:10.1016/j.diamond.2010.01.014

[22] Polcaro AM, Ricci PC, Palmas S, Ferrara F, Anedda A. Characterization of boron doped diamond electrodes during oxidation processes: Relationship between electrochemical activity and ageing time. Thin Solid Films 2006;515(4)2073-8. doi:10.1016/j.tsf.2006.06.033

[23] Hoffmann R, Kriele A, Obloh H, Hees J, Wolfer M, Smirnov W, et al. Electrochemical hydrogen termination of boron-doped diamond. Appl Phys Lett 2010;97:052103. http://dx.doi.org/10.1063/1.3476346

[24] Ryl J, Darowicki K. Impedance monitoring of carbon steel cavitation erosion under the influence of corrosive factors. J Electrochem Soc 2008;155(4)P44-9. doi: 10.1149/1.2840619

[25] Darowicki K, Orlikowski J, Arutunow A. Analysis of electrochemical parameters in time domain during the passive layer cracking occurring on the 304L stainless steel in chlorides solution under tensile stresses. Electrochim Acta 2004;49(28):5069-78. doi:10.1016/j.electacta.2004.05.045

[26] Krakowiak S, Darowicki K, Slepski P. Impedance of metastable pitting corrosion. J Electroanal Chem 2005;575(1):33-8. doi:10.1016/j.jelechem.2004.09.001

[27] Sobaszek M, Skowronski L, Bogdanowicz R, Siuzdak K, Cirocka A, Zieba P, et al. Optical and electrical properties of ultrathin transparent nanocrystalline boron-doped diamond electrodes. Opt Mater 2015;42:24-34. doi:10.1016/j.optmat.2014.12.014

[28] Fabianska A, Bogdanowicz R, Zieba P, Ossowski T, Gnyba M, Ryl J, et al. Electrochemical oxidation of sulfamerazine at boron-doped diamond electrodes: influence of boron concentration. Phys Status Solidi A 2013;210(10):2040-7. DOI: 10.1002/pssa.201300094

[29] Santana MHP, De Faria LA, Boodts JFC. Electrochemical characterization and oxygen evolution at a heavily boron doped diamond electrode. Electrochim Acta 2005;50(10):2017-27. doi:10.1016/j.electacta.2004.08.050

[30] Ferreira NG, Silva LLG, Corat EJ, Trava-Airoldi VJ. Kinetics study of diamond electrodes at different levels of boron doping as quasi-reversible systems. Diam Relat Mater 2002;11(8):1523-31. doi:10.1016/S0925-9635(02)00060-2

[31] Velicky M, Tam KY, Dryfe RAW. On the stability of the silver/silver sulfate reference electrode. Anal Methods 2012;4:1207-11. DOI: 10.1039/C2AY00011C

[32] Chaplin BP, Hubler DK, Farrell J. Understanding anodic wear at boron doped diamond film electrodes. Electrochim Acta 2013;89:122-31. doi:10.1016/j.electacta.2012.10.166

[33] Ryl J, Bogdanowicz R, Slepski P, Sobaszek M, Darowicki K. Dynamic electrochemical Impedance spectroscopy (DEIS) as a tool for analyzing surface oxidation processes on boron-doped diamond electrodes. J Electrochem Soc 2014;161(6):H359-64. doi: 10.1149/2.016406jes

[34] Darowicki K, Slepski P. Dynamic electrochemical impedance spectroscopy of the first order electrode reaction. J Electroanal Chem 2003;547(1):1-8. doi:10.1016/S0022-0728(03)00154-2

[35] Gioti M, Papadimitriou D, Logothetidis S. Optical properties and new vibrational modes in carbon films. Diam Relat Mater 2000;9(3-6):741-5. doi:10.1016/S0925-9635(00)00244-2

[36] Logothetidis S, Gioti M, Patasalas P, Charitidis C. Insights on the deposition mechanism on sputtered amorphous carbon films. Carbon 1999;37(5):765-9. doi:10.1016/S0008-6223(98)00268-1

[37] Jellison GE, Modine FA. Parameterization of the optical functions of amorphous materials on the interband region. Appl Phys Lett 1996;69:371-3. http://dx.doi.org/10.1063/1.118064

[38] Tompkins H, Irene EA. Handbook of Ellipsometry. 1st ed. New York: William; 2006.

[39] Orlikowski J, Ryl J, Jarzynka M, Krakowiak S, Darowicki K. Instantaneous impedance monitoring of aluminum alloy 7075 corrosion in borate buffer with admixed chloride ions. Corrosion 2015;71(7):828-38. http://dx.doi.org/10.5006/1546

[40] Ferro S, De Battisti A. Electron transfer reactions at conductive diamond electrodes. Electrochim Acta 2002;47(10):1641-9. doi:10.1016/S0013-4686(01)00898-2

[41] Granger MC, Swain GM. The influence of the surface interactions on the reversibility of ferri/ferrocyanide at boron-doped diamond thin-film electrodes. J Electrochem Soc 1999;146(12):4551-8. doi: 10.1149/1.1392673

[42] Robertson J. Electron field emission from diamond and diamond-like carbon for field emission displays. Carbon 1999;37(5):759-63. doi:10.1016/S0008-6223(98)00267-X

[43] Pleskov YV Evstefeeva YU, Varnin VP, Teremetskaya IG. Synthetic semiconductor diamond electrodes: electrochemical characteristics of homoepitaxial boron-doped films grown at the (111), (110), and (100) faces of diamond crystals. Russ J Electrochem+ 2004;40(9):886-92. doi:10.1023/B:RUEL.0000041354.70107.c8

[44] Ballutaud D, Simon N, Girard H, Rzepka E, Bouchet-Fabre B. Photoelectron spectroscopy of hydrogen at the polycrystalline diamond surface. Diam Relat Mater 2005;15(4-8):716-19. doi:10.1016/j.diamond.2006.01.004

[45] Charrier G, Levy S, Vigneron J, Etcheberry A, Simon N. Electroless oxidation of boron-doped diamond surface: comparison between four oxidizing agents; Ce^{4+}, MnO_4^-, H_2O_2 and $S_2O_8^{2-}$. Diam Relat Mater 2011;20(7):944-50. doi:10.1016/j.diamond.2011.05.003

[46] Wang M, Simon N, Charrier G, Bouttemy M, Etcheberry A, Li M, et al. Distinction between surface hydroxyl and ether groups on boron-doped diamond electrodes using a chemical approach. Electrochem Commun 2010;12(3):351-4. doi:10.1016/j.elecom.2009.12.029

[47] Ferrari AC, Robertson J. Origin of the 1150-cm^{-1} Raman mode in nanocrystalline diamond. Phys Rev B 2001;63:121405(R). http://dx.doi.org/10.1103/PhysRevB.63.121405

[48] Zeisel R, Nebel CE, Stutzmann M. Capacitance-voltage profiling of deuterium passivation and diffusion in diamond Schottky diodes. Diam Relat Mater 2000;9(3-6):413-6. doi:10.1016/S0925-9635(99)00260-5

[49] Zielinski A, Bogdanowicz R, Ryl J, Burczyk L, Darowicki K. Local impedance imaging of boron-doped polycrystalline diamond thin films. Appl Phys Lett 2014;105:131908. http://dx.doi.org/10.1063/1.4897346

[50] Ullah M, Ahmed E, Hussain F, Rana AM, Raza R. Electrical conductivity enhancement by boron-doped in diamond using first principle calculations. Appl Surf Sci 2015;334:40-4. doi:10.1016/j.apsusc.2014.07.157

[51] Krawiec H, Vignal V, Loch J, Erazmus-Vignal P. Influence of plastic deformation on the microstructural and corrosion behavior of Ti-10Mo-4Zr and Ti-6Al-4V alloys in the Ringer's solution at 37^{O}C. Corros Sci 2015;96:160-70. doi:10.1016/j.corsci.2015.04.006

[52] Pleskov YV, Evstefeeva YE, Krotova MD, Varnin VP Teremetskaya IG. Synthetic semiconductor diamond electrodes: electrochemical behavior of homoepitaxial boron-doped films oriented as (1 1 1), (1 1 0), and (1 0 0) faces. J Electroanal Chem 2006;595(2):168-74. doi:10.1016/j.jelechem.2006.07.010

[53] Wilson NR, Clewes SL, Newton ME, Unwin PR, Macpherson JV. Impact of grain-dependent boron uptake on the electrochemical and electrical properties of polycrystalline boron-doped diamond electrodes. J Phys Chem B 2006;110(11):5639-46. DOI: 10.1021/jp0547616

[54] Ostrovskaya L, Perevertailo V, Ralchenko V, Dementjev A, Loginova O. Wettability and surface energy of oxidized and hydrogen plasma-treatment diamond films. Diam Relat Mater 2002;11(3-6):845-50. doi:10.1016/S0925-9635(01)00636-7

[55] Ohmagari S, Srimongkon K, Yamada H, Umezawa H, Tsobouchi N, Chayahara A, et al. Low resistivity p^+ diamond (100) films fabricated by hot-filament chemical vapor deposition. Diam Relat Mater 2015;58:110-4. doi:10.1016/j.diamond.2015.06.011

[56] Zimmer A, Williams OA, Haenen K, Terryn H. Optical properties of heavily boron-doped nanocrystalline diamond films studied by spectroscopic ellipsometry. Appl Phys Lett 2008;93:131910. http://dx.doi.org/10.1063/1.2990679

[57] Gajewski W, Achatz P, Williams OA, Haenen K, Bustarret E, Stutzmann M, et al. Electronic and optical properties of boron-doped nanocrystalline diamond films. Phys Rev B 2009;79:045206. http://dx.doi.org/10.1103/PhysRevB.79.045206

[58] Wu D, Ma YC, Wang ZL, Luo Q, Gu CZ, Wang NL, et al. Optical properties of boron-doped diamond. Phys Rev B 2006;73:012501. http://dx.doi.org/10.1103/PhysRevB.73.012501

[59] Lasia A. Electrochemical Impedance Spectroscopy and its applications. Quebec: Springer Press; 2014.

[60] Elkin VV, Marshakov AI, Rybkina AA, Maleeva MA. Interpretation of the impedance comprising negative capacitance and constant phase element on iron electrode in weakly acid media. Russ J Electrochem+ 2011;47(2):134-46. DOI: 10.1134/S1023193511020054

[61] Duan X, O'Donnell K, Sun H, Wang Y, Wang S. Sulfur and nitrogen co-doped graphene for metal-free catalytic oxidation reaction. Small 2015;11(25):3036-44. DOI: 10.1002/smll.201403715

[62] Nomodo T, Yagi S, Soda K, Kutluk G, Sumida H, Hashimoto E, et al. Adsorption behavior of $(CH_3)_2S$ on sputtered and annealed Rh(100) surface by AFM, XPS and NEXAFS. J Surf Anal 2006;4:39-45. http://doi.org/10.1380/ejssnt.2006.39